VOL. 14, NO. 10, MAY 2019 ISSN 1819-6608
ARPN Journal of Engineering and Applied Sciences

www.arpnjournals.com

ELECTRIC AND MAGNETIC FIELDS ANALYSIS OF TRAVELING WAVE INDUCTION HEATING

Lina J. Rashad and Fadhil A. Hasan
Department of Electrical Engineering, University of Technology, Baghdad, Iraq
E-Mail: fadhil.a.hassan@gmail.com

ABSTRACT

The analysis of the electromagnetic problem is the dominant aspect to investigate the performance of the induction heating process. There are two universal analysis methods; the mathematical and numerical methods, each of them has its own advantages and drawbacks. This paper presents a comprehensive analysis of the electromagnetic problem, for the Traveling Wave Induction Heating (TWIH) system, by the aid of mathematical analytical approach. The 2-dimensional model is analyzed and the solution of the electromagnetic field is concern on investigation the behaviour of the magnetic field attenuation, material impedance, normal forces between the heater and material, the air gap flux, eddy current density, produced power, magnetizing reactance and effective workpiece resistance. The analytical results are verified by comparing them with that of the numerical analysis method. The comparison shows significant convergence between the presented analytical method and the numerical analysis method. The percentage errors between the two methods, for both of eddy current density and averaged power, are very acceptable for major analysis requirements. The proposed model can replace the numerical model in an efficient manner in terms of the accuracy of the results in addition to reducing the computation time and the provision of effort in building the numerical model.

Keywords: induction heating, Mathematical analysis, traveling wave induction heating, eddy current density.

INTRODUCTION

Generally, there are two main solving methods for the electromagnetic problem in the Traveling Wave Induction Heating (TWIH) systems; the analytical (mathematical) solution, and numerical solution [1]. The numerical method is a global analysis tool in the investigation of the TWIH performance, but this method suffers from specific limitation such as; the long computational time, and the computation program doesn't give a general solution but presents an analytical solution for a particular case. Also, the heated workpiece parameters may vary from bath to bath during the heating process (such as material type and thickness) [2]. In other words, for each case, it's required a different analytical process and hence different finite element model. For these reasons, the mathematical model of the TWIH becomes essential in this work.

Physically, the skin effect is an important factor which describes the rapid decreasing of the induced currents with the penetration in the material. Eddy currents tend to be concentrated on the surface of the material, it results that the power and therefore the heat is mainly dissipated on the surface. This skin effect is largely depending on the frequency and the properties of the workpiece. The skin effect is characterized by a certain thickness, called "penetration depth δ", which theoretically expressed by equation (1).

$$\delta = \sqrt{\frac{\rho}{\pi f \mu_o \mu_r}} \quad (1)$$

Where ρ is the resistivity of the material, f is the frequency, μ_o permeability of the free space, μ_r is the relative permeability.

About 63% of the eddy current density is flows within the penetration depth. Thus, in IH about 87% of the heat is generated within this region [3], as shown in Figure-1, hence the time required for heating is much shorter than that of fuel-fired furnaces. When the workpiece is flat such as; strip, plate or thin slab (i.e. the width is much more than the thickness), insufficient magnetic flux intercepted to induce a useful amount of heat, and effective heating is only possible if high-frequency fields are used. This entails unacceptably high capital cost equipment, low overall efficiency and very large temperature differentials between the surface and the workpiece centre, leading to unacceptably temperature distribution through the workpiece [4].

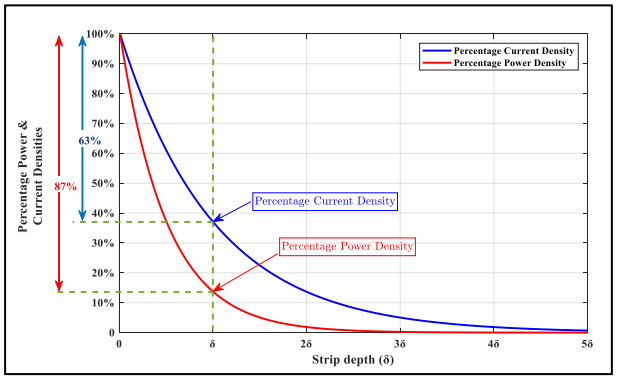

Figure-1. The effect of skin depth on the current and power densities.

To overcome these problems in IH of a flat workpiece, the induction coil is arranged so that the magnetic flux passes through the workpiece perpendicular to its surface. This produces induced eddy currents which circulate in the plane of the workpiece, more magnetic

flux intercepts the workpiece, inducing higher voltages and, in turn, bigger currents and rapid heating of the workpiece. There are several methods of heating flat materials; the most efficient method is the Traveling Wave Induction Heating (TWIH).

In this paper, the mathematical modelling and analysis, of the TWIH system, are presented in a two-dimensional model to investigate the electromagnetic field quantities for both of the heater and heated workpiece. By the 2-D model, the conception of the TWIH theory can be derived by determination of the electromagnetic field quantities within the heating system. The solution of the electromagnetic field is concern on investigation the behaviour of the magnetic field attenuation, material impedance, normal forces between the heater and material, the air gap flux, eddy current density, produced power, magnetizing reactance and effective workpiece resistance.

INITIAL ASSUMPTIONS

The analysis of the electromagnetic phenomena is based on Maxwell's equations. This analysis assumes that the system is magnetically linear. The TWIH analysis using the magnetic vector potential [5, 6], from which the various field quantities are derived. Solutions are obtained for the electromagnetic field distribution in various heating regions; coils, airgap and workpiece. Figure-2 shows the selected model for analysis and the associated coordinate system.

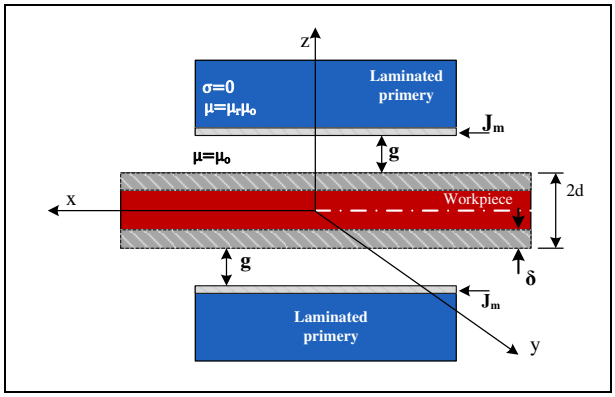

Figure-2. The two-dimensional model of the TWIH.

In order to reduce the complexity of the analysis, some assumptions, are taken into account, which is convenient for electrical machine analysis [7, 8]:

a) The physical parameters of the materials are homogeneous, isotropic and linear.
b) The material is magnetically unsaturated.
c) The coil current is assumed to be current sheets in the y-direction located on the surface of the primary core.
d) All y-direction of the magnetic field quantities is ignored.
e) The conductivity of the primary core is neglected by laminated the core in the x-direction.
f) The variation of the electromagnetic field quantities in time and space are assumed to be harmonics.
g) The dimension of the heater is extended to infinity in both x- and y-direction.

Points 1 to 3 made for linear behaviour, points 4 and 5 are used to reduce the analysis dimension and complexity. Point 6 is valid because the supply voltage and current are sinusoidal, and ideally distributed of the primary winding leads to the sinusoidal magnetic field. Point 7 is made to cancel the edge and end turn effects from the analysis.

Electromagnetic fields analysis

The Maxwell's equations are:

$$\nabla . \mathrm{B} = 0 \tag{2}$$

$$\nabla \times \mathrm{H} = \mathrm{J} + \frac{\partial \mathrm{D}}{\partial \mathrm{t}} \tag{3}$$

$$\nabla \times \mathrm{E} = -\frac{\partial \mathrm{B}}{\partial \mathrm{t}} \tag{4}$$

$$\mathrm{J} = \sigma \mathrm{E} \tag{5}$$

Where: **B** is the magnetic field density, **H** is the magnetic field intensity, **J** is the current density, **D** is the electric field density, **E** is the electric field intensity, **σ** is the media conductivity.
Note: the bold letters refers to vector quantities.

The current sheets are assumed to be located of the surface of the two primaries. The current flows in the y-direction only and its line density (A/m) is represented by [8]:

$$\mathrm{J_y} = \mathrm{J_m}\, e^{\mathrm{j}(\omega \mathrm{t} - \beta \mathrm{x})} \tag{6}$$

Where: $\mathrm{J_m}$ is the maximum value of the current density, ω is the angular frequency, β is the phase constant.

Since the displacement current density at low frequency is neglected i.e. $\frac{\partial \mathbf{D}}{\partial \mathrm{t}} = 0$; Equation (3) becomes:

$$\nabla \times \mathrm{H} = \mathrm{J} \tag{7}$$

Substitute (7) in (5) and $B = \mu H$ obtain:

$$\nabla \times \mathrm{B} = \mu \sigma \mathrm{E} \tag{8}$$

Where μ is the permeability of the media.

The magnetic vector potential (A) is defined as [5, 6]:

$$\nabla \times \mathrm{A} = \mathrm{B} \tag{9}$$

From equations (8) and (9):

$$\nabla \times \nabla \times \mathrm{A} = \mu \sigma \mathrm{E} \tag{10}$$

$$\nabla . (\nabla . \mathrm{A}) - \nabla^2 \mathrm{A} = \mu \sigma (-\partial \mathrm{A}/\partial \mathrm{t}) \tag{11}$$

$$\nabla . \mathrm{A} = 0$$

$$\nabla^2 \mathrm{A} = \mu\sigma(\partial \mathrm{A}/\partial \mathrm{t}) \quad (12)$$

The excitation current produces only z-direction traveling field density at the pole face which travels in the x-direction:

$$\mathrm{B_z} = \mathrm{B_m}\, e^{\mathrm{j}(\omega \mathrm{t} - \beta \mathrm{x})} \quad (13)$$

Since (A) is assumed in y-direction and is not function of (y):

$$\mathrm{A_y} = \mathrm{A_{(z)}}\, e^{\mathrm{j}(\omega \mathrm{t} - \beta \mathrm{x})} \quad (14)$$

Therefore, equation (12) yields to:

$$\frac{\partial^2 A_y}{\partial x^2} + \frac{\partial^2 A_y}{\partial z^2} = j\omega\sigma\mu A_y \quad (15)$$

While, in the airgap region:

$$\frac{\partial^2 A_y}{\partial x^2} + \frac{\partial^2 A_y}{\partial z^2} = 0 \quad (16)$$

From equation (14):

$$\frac{\partial A_y}{\partial x} = -j\beta A_{(z)}\, e^{j(\omega t - \beta x)} \quad (17)$$

$$\frac{\partial^2 A_y}{\partial x^2} = -\beta^2 A_{(z)}\, e^{j(\omega t - \beta x)} \quad (18)$$

Substitute equation (18) into (15) yields:

In the workpiece region:

$$\frac{\partial^2 \boldsymbol{A_y}}{\partial z^2} - \beta^2 \boldsymbol{A_y} = j\omega\sigma\mu \boldsymbol{A_y} \quad (19)$$

And for the airgap region:

$$\frac{\partial^2 \boldsymbol{A_y}}{\partial z^2} - \beta^2 \boldsymbol{A_y} = 0 \quad (20)$$

Since the propagation constant γ equal to:

$$\gamma = \sqrt{\beta^2 + j\omega\mu\sigma} \quad (21)$$

Equation (19) becomes:

$$\frac{\partial^2 \boldsymbol{A_y}}{\partial z^2} - \gamma^2 \boldsymbol{A_y} = 0 \quad (22)$$

The solutions of these second order differential equations (20) and (22) are:
Workpiece:

$$A_{y(w)} = \big(Acosh(\gamma z) + Bsinh(\gamma z)\big).\, e^{j(\omega t - \beta x)} \quad (23)$$

Airgap:

$$A_{y(a)} = \big(Ccosh(\beta z) + Dsinh(\beta z)\big).\, e^{j(\omega t - \beta x)} \quad (24)$$

$$\mathrm{B} = \nabla \times \mathrm{A} = \begin{bmatrix} \mathrm{a_x} & \mathrm{a_y} & \mathrm{a_z} \\ \frac{\partial}{\partial x} & \frac{\partial}{\partial y} & \frac{\partial}{\partial z} \\ 0 & A_y & 0 \end{bmatrix} = -a_x \frac{\partial A_y}{\partial z} + a_z \frac{\partial A_y}{\partial x}$$

$$B_{x(w)} = -\gamma\big(Asinh(\gamma z) + Bcosh(\gamma z)\big).\, e^{j(\omega t - \beta x)} \quad (25)$$

$$B_{z(w)} = -j\beta\big(Acosh(\gamma z) + Bsinh(\gamma z)\big).\, e^{j(\omega t - \beta x)} \quad (26)$$

$$H_{x(w)} = -\frac{\gamma}{\mu}\big(Asinh(\gamma z) + Bcosh(\gamma z)\big).\, e^{j(\omega t - \beta x)} \quad (27)$$

$$H_{z(w)} = -j\frac{\beta}{\mu}\big(Acosh(\gamma z) + Bsinh(\gamma z)\big).\, e^{j(\omega t - \beta x)} \quad (28)$$

Similarly, the airgap magnetic fields are:

$$B_{x(a)} = -\beta\big(Csinh(\beta z) + Dcosh(\beta z)\big).\, e^{j(\omega t - \beta x)} \quad (29)$$

$$B_{z(a)} = -j\beta\big(Ccosh(\beta z) + Dsinh(\beta z)\big).\, e^{j(\omega t - \beta x)} \quad (30)$$

$$H_{x(a)} = -\frac{\beta}{\mu o}\big(Csinh(\beta z) + Dcosh(\beta z)\big).\, e^{j(\omega t - \beta x)} \quad (31)$$

$$H_{z(a)} = -j\frac{\beta}{\mu o}\big(Ccosh(\beta z) + Dsinh(\beta z)\big).\, e^{j(\omega t - \beta x)} \quad (32)$$

In the other hand the electric field intensity are [9]:

$$\mathrm{E} = \frac{1}{\mu\sigma}\nabla \times \mathrm{B} = \begin{bmatrix} \mathrm{a_x} & \mathrm{a_y} & \mathrm{a_z} \\ \frac{\partial}{\partial x} & \frac{\partial}{\partial y} & \frac{\partial}{\partial z} \\ B_x & 0 & B_z \end{bmatrix} = a_x \frac{\partial B_z}{\partial y} - a_y \left(\frac{\partial B_z}{\partial x} - \frac{\partial B_x}{\partial z}\right) - a_z \frac{\partial B_x}{\partial y}$$

$$E_{y(w)} = -j\omega\big(Acosh(\gamma z) + Bsinh(\gamma z)\big).\, e^{j(\omega t - \beta x)} \quad (33a)$$

For airgap the following relation can be used:

$$\nabla \times \mathrm{E} = \begin{bmatrix} \mathrm{a_x} & \mathrm{a_y} & \mathrm{a_z} \\ \frac{\partial}{\partial x} & \frac{\partial}{\partial y} & \frac{\partial}{\partial z} \\ E_x & E_y & E_z \end{bmatrix} = -j\omega\mu_o \mathrm{H}$$

$$\left(\frac{\partial E_z}{\partial y} - \frac{\partial E_y}{\partial z}\right) a_x - \left(\frac{\partial E_z}{\partial x} - \frac{\partial E_x}{\partial z}\right) a_y + \left(\frac{\partial E_y}{\partial x} - \frac{\partial E_x}{\partial y}\right) a_z = -j\omega\mu_o (H_x + H_y + H_z)$$

Since $H_y = 0$, then:

$$-j\omega\mu_o H_x = \left(\frac{\partial E_z}{\partial y} - \frac{\partial E_y}{\partial z}\right) \overset{\frac{\partial E_z}{\partial y}=0}{\Longrightarrow} -j\omega\mu_o H_x = \left(-\frac{\partial E_y}{\partial z}\right)$$

$$-j\omega\mu_o H_z = \left(\frac{\partial E_y}{\partial x} - \frac{\partial E_x}{\partial y}\right) \overset{\frac{\partial E_x}{\partial y}=0}{\Longrightarrow} -j\omega\mu_o H_z = \left(\frac{\partial E_y}{\partial x}\right)$$

$$E_{y(a)} = -j\omega\big(Ccosh(\beta z) + Dsinh(\beta z)\big).\, e^{j(\omega t - \beta x)} \quad (33b)$$

By applying the boundary conditions of this problem the constants of the final solutions can be obtained as:

$$A = \frac{B_m}{-jcosh(\gamma d)\,(\gamma tanh(\gamma d)\ \sinh(\beta g) + \beta\cosh(\beta g))} \quad (34)$$

$$B = 0 \quad (35)$$

$$C = \frac{B_m(\gamma\, tanh(\gamma d)\, sinh(\beta d) - \beta\, cosh(\beta d))}{j\beta\,(\gamma tanh(\gamma d)\ sinh(\beta g) + \beta\, cosh(\beta g))} \quad (36)$$

$$D = \frac{B_m(\beta\, sinh(\beta d) - \gamma\, tanh(\gamma d)\, cosh(\beta d))}{j\beta\,(\gamma tanh(\gamma d)\ sinh(\beta g) + \beta\, cosh(\beta g))} \quad (37)$$

The performance of the normal and tangential magnetic field intensity are shown in Figures (3) and (4) respectively. And the distribution of the electric field intensity is shown in Figure-5.

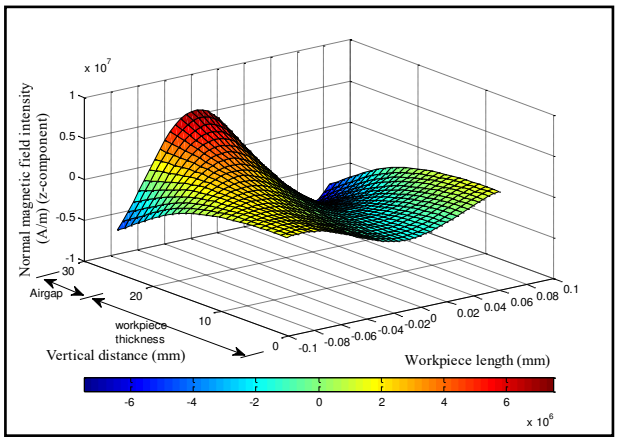

Figure-3. The normal magnetic field intensity.

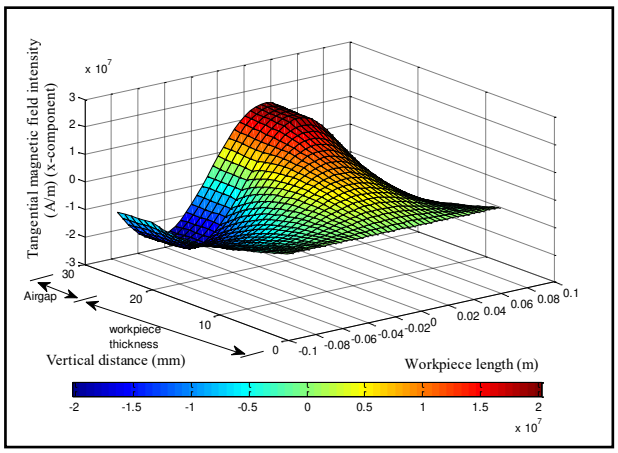

Figure-4. The tangential magnetic field intensity.

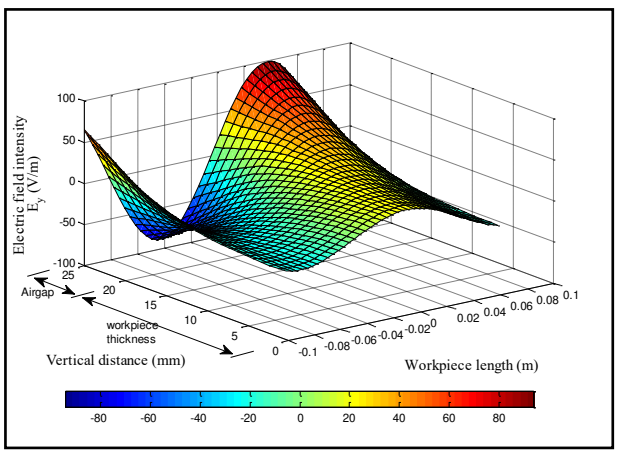

Figure-5. The electric field intensity.

Magnetic field attenuation

The attenuation of the magnetic field components inside the workpiece can be derived from the solution of the magnetic field as follow:

The x-component of the magnetic flux density is obtained from equation (25):

$$B_{x(w)} = -\gamma A\, sinh(\gamma z).\, e^{j(\omega t - \beta x)} \quad (38)$$

Substitute equation (34) into (38) gives:

$$B_{x(w)} = \frac{B_m \gamma\, sinh(\gamma z).e^{j(\omega t-\beta x)}}{j cosh(\gamma d)\,(\gamma tanh(\gamma d)\ \sinh(\beta g) + \beta\cosh(\beta g))} \quad (39)$$

On the workpiece surface (z=d), the x-component of the magnetic flux density becomes:

$$B_{x(w)} = \frac{B_m \gamma\, tanh(\gamma d).e^{j(\omega t-\beta x)}}{j\,(\gamma tanh(\gamma d)\ \sinh(\beta g) + \beta\cosh(\beta g))} \quad (40)$$

In the other hand the z-component of the magnetic flux density in the workpiece can be obtained from equation (26):

$$B_{z(w)} = -j\beta A\, cosh(\gamma z)\,.\, e^{j(\omega t-\beta x)} \quad (41)$$

Substitute equation (34) into (35) gives:

$$B_{z(w)} = \frac{B_m \beta\, cosh(\gamma z).e^{j(\omega t-\beta x)}}{cosh(\gamma d)\,(\gamma tanh(\gamma d)\ \sinh(\beta g) + \beta\cosh(\beta g))} \quad (42)$$

Again, on the surface of the workpiece (z=d) equation (42) can be reduced to:

$$B_{z(w)} = \frac{B_m\, \beta\, .e^{j(\omega t-\beta x)}}{(\gamma tanh(\gamma d)\ \sinh(\beta g) + \beta\cosh(\beta g))} \quad (43)$$

Equations (40) and (43) represent the x- and z-components of the magnetic flux density on the workpiece surface. These equations can be more simplified if the term (βg) is very small and assumed to be equal to zero (this is true if the air gap does not exceed 2% of the heater pole pitch) [10], from this assumption these equations become at the surface of the workpiece:

$$B_{x(w)} = \frac{\gamma\, B_m\, tanh(\gamma d).e^{j(\omega t-\beta x)}}{j\beta} \quad (44)$$

$$B_{z(w)} = B_m.\, e^{j(\omega t-\beta x)} \quad (45)$$

From these equations, it may be noticed that the tangential component (x-component) of the magnetic flux density is proportion directly to the primary coil excitation, as well as heater parameters, supply frequency and physical properties of the heated material, such as electrical conductivity and magnetic permeability. It's important to mention here that the tangential component of the magnetic flux density is the dominant component on the workpiece surface. While the normal component (z-component) of the magnetic flux density on the workpiece

surface depends largely on the primary coil excitation current.

Characteristic impedance of the workpiece

The characteristic impedance of the workpiece is the main important parameter in the equivalent circuit, which is a very effective tool in the study of the TWIH performance and design parameters. From the solution of the electromagnetic field quantities in the two-dimensional model, the unit surface impedance of the workpiece can be obtained from the ratio of the tangential component of electric to magnetic fields intensity [7, 10].

$$Z_z = \frac{E_{y(w)}}{H_{x(w)}}\Big|_{z=d} \quad (46)$$

Substitute equation (27) and (33) into (46):

$$Z_z = \frac{-j\omega\left(A\cosh(\gamma d)+B\sinh(\gamma d)\right).e^{j(\omega t-\beta x)}}{-\frac{\gamma}{\mu}\left(A\sinh(\gamma d)+B\cosh(\gamma d)\right).e^{j(\omega t-\beta x)}} \quad (47)$$

Since B = 0:

$$Z_z = \frac{j\omega\left(\cosh(\gamma d)\right)}{\frac{\gamma}{\mu}\left(\sinh(\gamma d)\right)} \quad (48)$$

$$Z_z = \frac{j\omega\mu}{\gamma}\ coth(\gamma d);\ Or\ \frac{j\omega\mu}{\gamma\ tanh(\gamma d)} \quad (49)$$

From this equation the term $tanh(\gamma d)$falls down to zero, as workpiece thickness decreases, this means that the workpiece impedance increases with the reduction of its thickness.

Eddy current density

The induced eddy current density in the workpiece can be obtained by [6, 8]:

$$J_{y(w)} = \sigma E_{y(w)}$$
$$J_{y(w)} = -j\sigma\omega\left(A\ cosh(\gamma z)\right).e^{j(\omega t-\beta x)} \quad (50)$$

Substitute the value of (A) in equation (50):

$$J_{y(w)} = \frac{-\omega\ \sigma\ B_m\ cosh(\gamma z).e^{j(\omega t-\beta x)}}{cosh(\gamma d)\ (\gamma tanh(\gamma d)\ \sinh(\beta g)+\beta\cosh(\beta g))} \quad (51)$$

On the surface of the workpiece (z=d), equation (51) becomes:

$$J_{y(\omega)} = \frac{-\omega\ \sigma\ B_m\ .e^{j(\omega t-\beta x)}}{(\gamma\ tanh(\gamma d)\ \sinh(\beta g)+\beta\cosh(\beta g))} \quad (52)$$

By assuming the term (βg) is equal to zero, because it is very small, equation (52) becomes:

$$J_{y(\omega)} = \frac{-\omega\ \sigma\ B_m\ .e^{j(\omega t-\beta x)}}{\beta} \quad (53)$$

The performance of the eddy current within the workpiece is shown in Figure (6):

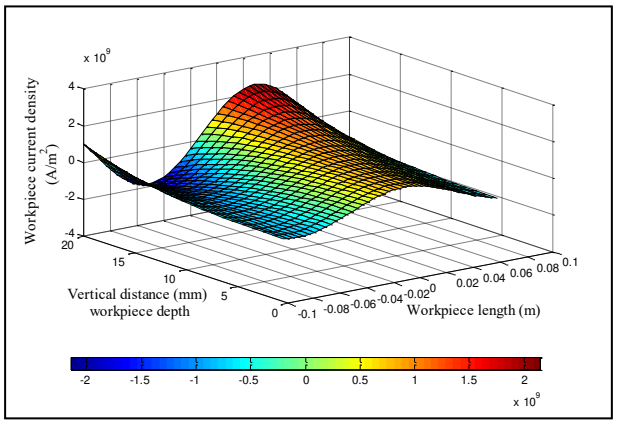

Figure-6. The eddy current distribution.

Power producing and thrust force

The power produced within the workpiece and the thrust force can be derived from the solution of the electromagnetic field quantities in the two-dimensional model:

$$f_x = \mathrm{a_x}.(\mathrm{J}\times\mathrm{B}) = J_{y(w)}B_{z(w)} \quad (54)$$

Where $\mathbf{a_x}$ denotes a unit vector in the x-direction. If $J_{y(w)}\ and\ B_{z(w)}$ are written in a complex form, the time average force density is [7, 10]:

$$f_x = \tfrac{1}{2}\,Real\,[J_{y(w)}B_{z(w)}] \quad (\mathrm{N/m^3}) \quad (55)$$

Substitute equation

$$f_x = \frac{1}{2}\frac{\omega\sigma\beta\ B_m^2|cosh(\gamma z)|^2}{|cosh(\gamma d)|^2\ |\gamma tanh(\gamma d)\ sinh(\beta g)+\beta\ cosh(\beta g)|^2} \quad (56)$$

The thrust force is:

$$F_x = \int_0^d\int_{-w_c/2}^{w_c/2}\int_0^{P\lambda} f_x\ \ dx\ dy\ dz\ \ (\mathrm{N}) \quad (57)$$

By using the mathematical relation:

$$|cosh(\gamma z)|^2 = \frac{1}{2}[cosh(2rz)+cos(2sz)] \quad (58)$$

$$\mathrm{F_x} = \frac{\mathrm{P\lambda\ w_c\ \omega\ \sigma\ \beta\ B_m^2}\left\{\frac{\sinh(2rd)}{2r}+\frac{\sin(2sd)}{2s}\right\}}{2\ |\gamma\tanh(\gamma d)\ \sinh(\beta g)+\beta\cosh(\beta g)|^2\{\cosh(2rd)+\cos(2sd)\}}\ (\mathrm{N}) \quad (59)$$

The variation of the thrust force within the workpiece, for different airgap values, is shown in Figure-7:

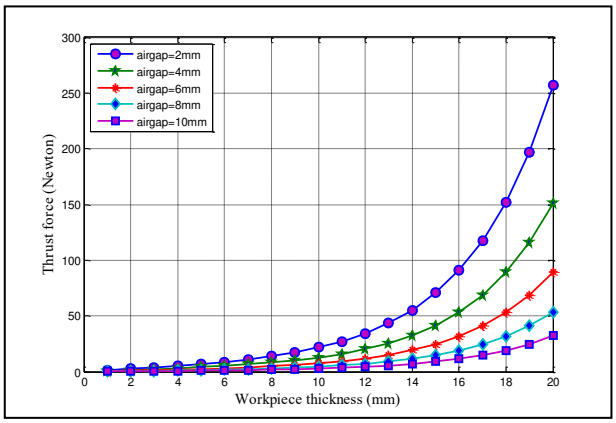

Figure-7. The thrust force of the workpiece.

The workpiece power density can be obtained by:

$$p_w = Real(J_{y(w)}E_{y(w)}), \quad \text{or} \quad p_w = \frac{(Real(J_{y(w)}))^2}{\sigma}(\text{W/m}^3) \qquad (60)$$

$$\mathrm{p_w} = \sigma \left| \frac{\omega\, \mathrm{B_m}\, \cosh(\gamma z)}{\cosh(\gamma d)\,(\gamma \tanh(\gamma d)\, \sinh(\beta g)+\beta \cosh(\beta g))} \right|^2 (\text{W/m}^3) \qquad (61)$$

The performance of the producing power density within the workpiece is shown in Figure-8:

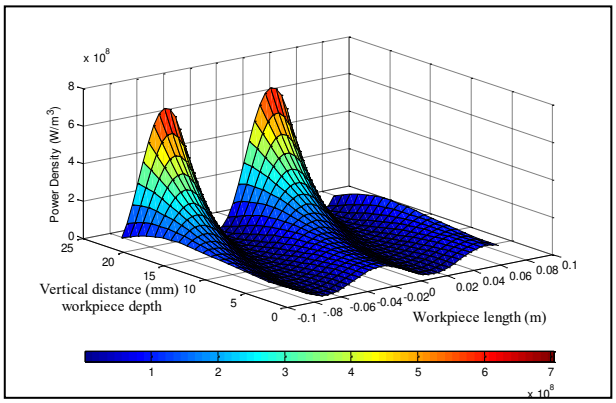

Figure-8. The producing power in the workpiece.

The power lost within the workpiece:

$$P_x = \int_0^d \int_{-w_c/2}^{w_c/2} \int_0^{P\lambda} p_x \quad dx\, dy\, dz \qquad (62)$$

$$P_w = \frac{P\lambda^2\, w_c\, \omega\, f\, \sigma\, \beta\, B_m^2 \left\{\frac{sinh(2rd)}{2r}+\frac{sin(2sd)}{2s}\right\}}{|\gamma tanh(\gamma d)\ sinh(\beta g)+\beta\, cosh(\beta g)|^2\{cosh(2rd)+cos(2sd)\}} \qquad (63)$$

Normal force

The normal force F_n between the primary core of the TWIH and the workpiece can be found as follows:
The normal force density [10]:

$$f_n = \mathrm{a_z}.(\mathrm{J} \times \mathrm{B}) = -J_{y(w)}B_{x(w)} \qquad (64)$$

Where $\mathrm{a_z}$ denotes a unit vector in the z-direction.
The time average force density is:

$$f_n = \frac{-1}{2} Real\,[J_{y(w)}B_{x(w)}] \quad (\text{N/m}^3) \qquad (65)$$

Substitute equations

$$f_n = \frac{-1}{2} \frac{\omega\, \sigma\, B_m^2\ Real\,(-\gamma\, sinh(\gamma z)\cosh(\gamma z))}{|cosh(\gamma d)|^2\ |\gamma\, tanh(\gamma d)\ \sinh(\beta g)+\beta \cosh(\beta g)|^2} \qquad (66)$$

The normal force is:

$$F_n = \int_0^d \int_{-w_c/2}^{w_c/2} \int_0^{P\lambda} f_{nr} \quad dx\, dy\, dz \quad (\text{N}) \qquad (67)$$

$$F_n = \frac{1}{2} \frac{P\lambda\, w_c\, \omega\, \sigma\, B_m^2\, [-r^2\cosh(2rd)-s^2\cosh(2rd)+r^2+s^2]}{2rs|cosh(\gamma d)|^2\ |\gamma\, tanh(\gamma d)\ \sinh(\beta g)+\beta \cosh(\beta g)|^2} \qquad (68)$$

If the net normal force becomes negative, this means that the force is repulsive, and this case occurs in nonmagnetic materials. Whereas, if the force is positive this means that the force is attractive, and this occurs in magnetic materials, as shown in Figure-9.

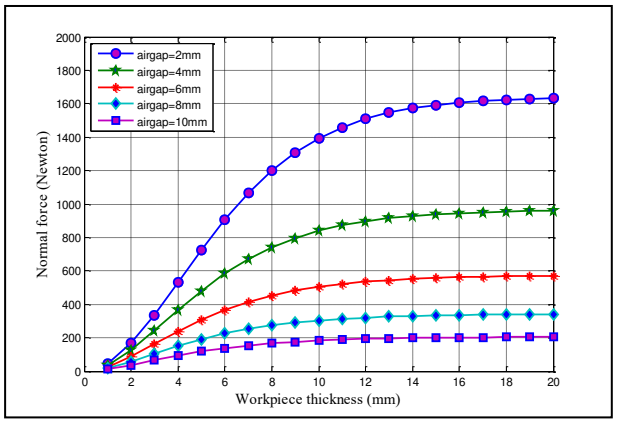

Figure-9. The normal force on the workpiece.

Magnetizing reactance

The unit impedance looking from a primary current sheet into the region below the current sheet represents the unit magnetizing reactance in parallel with the unit workpiece surface impedance, and can be obtained as follows:

$$Z_s = \left.\frac{E_{y(a)}}{H_{x(a)}}\right|_{z=d+g} \qquad (69)$$

Substitute equations (33) and (31) into (69) to get:

$$Z_s = \frac{-j\omega(Ccosh(\beta(d+g))+Dsinh(\beta(d+g))).e^{j(\omega t-\beta x)}}{-\frac{\beta}{\mu o}(Csinh(\beta(d+g))+Dcosh(\beta(d+g))).e^{j(\omega t-\beta x)}} \qquad (70)$$

Substitute equations (45) and (46) into (70):

$$Z_s = \frac{-j\omega\mu_o}{\beta}\left[\frac{e^{-\beta g}-e^{\beta g}\frac{(\gamma\tanh(\gamma d)+\beta)}{(\gamma\tanh(\gamma d)-\beta)}}{e^{-\beta g}+e^{\beta g}\frac{(\gamma\tanh(\gamma d)+\beta)}{(\gamma\tanh(\gamma d)-\beta)}}\right] \qquad (71)$$

Equation (71) represents the unit workpiece impedance Z_z in parallel with the unit magnetizing reactance X_s as:

$$Z_s = \frac{X_s.Z_z}{X_s+Z_z} \quad (72)$$

To find X_s from equation (72), Z_z must approach infinity and this condition occurs in equation (49) when the term $(tanh(\gamma d))$ approaches to zero, substitute this condition into equation (71) gives:

$$X_s = \frac{-j\omega\mu_o}{\beta tanh(\beta g)} \quad (73)$$

Maximum airgap flux density

The maximum airgap flux density, neglecting edge and end turn effects, can be determined as follows: The air gap flux density as assumed in equation (13):

$$B_z = B_m\, e^{j(\omega t-\beta x)}$$

The magnetic flux per pole can be obtained by integrating the flux density across the pole area as:

$$\psi = \int_{-w_c/2}^{w_c/2}\int_0^{P\lambda} B_z\, dx\, dy \quad (74)$$

$$\psi = \int_{-w_c/2}^{w_c/2}\int_0^{P\lambda} B_m\, e^{j(\omega t-\beta x)}\, dx\, dy \quad (75)$$

$$= -j\frac{2\lambda w_c B_m}{\pi} e^{j\omega t} \quad (76)$$

From Faraday's law; the induced back e.m.f per single turn is:

$$e = -\frac{d\psi}{dt} = -j\omega\psi \quad (77)$$

Substitute equation (76) into (77) to get:

$$e = -\frac{2\omega w_c \lambda B_m}{\pi}\, e^{j\omega t} \quad (78)$$

The r.m.s value of the back e.m.f per phase is:

$$E_{ph} = -2\sqrt{2} f w_c \lambda N_{ph} K_w B_m \quad (79)$$

Where N_{ph} denotes the number of turns per phase, $K_w$denotes the winding factor and the negative sign indicates the direction of the back e.m.f with respect to the original cause (Linz's theory).

$$\overset{Then}{\Longrightarrow} B_m = \frac{E_{ph}}{2\sqrt{2}\, f\, w_c\, \lambda\, N_{ph} K_w} \quad (80)$$

Also, the maximum air gap flux density can be derived from Maxwell's equations as an alternative method.

Workpiece thickness criterion

In the expressions of the workpiece impedance in equation (49), minimum impedance occurs when the term $(tanh(\gamma d))$ approaches unity, this happen when the term:

$$|\gamma d| \geq 2.5 \quad (81)$$

From this equation the critical thickness of the workpiece is:

$$d_c = \frac{2.5}{|\gamma|} \quad (82)$$

$$or\ d_c \approx \frac{2.5}{\sqrt{\pi f \mu \sigma}} \quad \text{(For high conducting material)} \quad (83)$$

$$or\ d_c = 2.5 \times \delta \quad (84)$$

Where d_c denotes the critical thickness of the half workpiece.

The critical thickness depends on the physical properties of the workpiece material such as the electrical conductivity and the magnetic permeability as well as the supply frequency.

Physically, if the workpiece thickness is less than critical thickness $(\frac{d}{\delta} \leq 2.5)$ the magnetic field will flow across the workpiece thickness, resulting in a lower reaction field, lower x-component of magnetic field intensity at the workpiece surface and higher workpiece impedance. And hence induced lower workpiece current, but due to the higher workpiece effective resistance, the workpiece power will be higher and, hence, perform higher heater efficiency.

If the workpiece thickness is greater than the critical thickness $(\frac{d}{\delta} > 2.5)$, the magnetic field will attenuate inside the workpiece rapidly before reaching the workpiece centre, at an approximate depth of (2.5δ).

Effective workpiece resistance

The equivalent circuit technique is a simple and approximate tool in the analysis of the TWIH, for design and performance calculations. The equivalent circuit construction is based on the per-phase per-heater side. From the similarity between TWIH with thick workpiece, and the solid core when subjected to an alternating magnetic field, the methods of the core impedance calculation can be applied to calculate the workpiece surface impedance, and hence, by referring this surface impedance (which is the important parameter in the equivalent circuit) to the coil side, as well as referring the magnetizing reactance, the equivalent circuit can be developed.

The magnetizing reactance can be derived from the conventional AC machine theory, by neglecting any saturation, while the per-phase coil resistance and leakage reactance can be adopted from the linear AC machine theory. From the equivalent circuit of the TWIH and the solution of the magnetic field in a two-dimensional model,

an effective workpiece resistance can be derived as follows:

The workpiece resistance R_w can be obtained as:

$$R_w = \frac{P_w}{3I_w^2} = \frac{P_w}{3\frac{|E_{ph}|^2}{|Z_l|^2}} \quad (85)$$

The normal component of the magnetic flux density in the air gap between the primary core surface and the workpiece surface, neglecting saturation and the end effects, given in equation (13):

$$B_z = B_m\, e^{j(\omega t - \beta x)}$$

$$B_m = \frac{\mu_o \lambda J_m}{\pi g} \quad (86)$$

Where $J_m$denotes the current sheet density (A/m) on the primary surface.

The r.m.s value of the induced e.m.f per phase in equation (79):

$$E_{ph} = -2\sqrt{2} f w_c \lambda N_{ph} K_w B_m$$

Also, Maxwell's equation$\nabla \times E = -\partial B/\partial t$, in the air gap, can be simplified as follows:

$$\frac{\partial E_y}{\partial x} = -\frac{\partial B_z}{\partial t} \quad (87)$$

$$\frac{\partial E_y}{\partial x} = -j\omega B_z \quad (88)$$

$$\frac{\partial E_y}{\partial x} = -j\omega B_m e^{j(\omega t - \beta x)} \quad (89)$$

Integrating both sides of equation (89) to obtain:

$$E_y = \frac{\omega B_m e^{j(\omega t - \beta x)}}{\beta} \quad (90)$$

$$E_m = \frac{\omega B_m}{\beta} \quad (91)$$

$$B_m = \frac{\beta E_m}{\omega} \quad (92)$$

Substitute (92) into (79) to get:

$$E_{ph} = \frac{-2\sqrt{2} f w_c \lambda N_{ph} K_w \beta E_m}{\omega} = \frac{-\sqrt{2} w_c \lambda N_{ph} K_w \beta E_m}{\pi} \quad (93)$$

The M.M.F required to sustain the load current (workpiece current referred to the primary coil side) per pole is given from the AC machine theory as [10]:

$$M.M.F = \frac{2\sqrt{2}\, m\, N_{ph} K_w I_l}{P\, \pi} \quad (94)$$

Where *m* is the phase number.

In an alternative form, the M.M.F can be obtained as [10]:

$$M.M.F = \lambda H_m \quad (95)$$

Equating equations (94) and (95) to get:

$$I_l = \frac{P\, \pi\, \lambda\, H_m}{2\sqrt{2}\, m\, N_{ph} K_w} \quad (96)$$

The workpiece impedance referred to the primary coil side can be obtained as:

$$Z_l = \frac{E_{ph}}{I_l} \quad (97)$$

Substitute equations (93) and (96) into equation (97) gives:

$$Z_l = \frac{-4 m w_c (N_{ph} K_w)^2}{P\, \pi\, \lambda} \cdot \frac{E_m}{H_m} \quad (98)$$

Substitute equation (78) into (98) to get:

$$Z_l = K_s \cdot Z_s \quad (99)$$

Where $K_s = \frac{-4 m w_c (N_{ph} K_w)^2}{P\, \pi\, \lambda}$ is the heater constant.
Substitute equations (99) and (93) into (85) to obtain:

$$R_w = \frac{4\rho_s K_s r^2 s^2 d}{(r^2+s^2)} \cdot \frac{\left[\frac{sinh(2rd)}{2r} + \frac{sin(2sd)}{2s}\right]}{[cosh(2rd) - cos(2sd)]} \quad (100)$$

Where $(\rho_s K_s)$ is the dc resistance of the workpiece referred to the primary side. And the term: $\left\{\frac{4\, r^2 s^2 d}{(r^2+s^2)} \cdot \frac{\left[\frac{sinh(2rd)}{2r} + \frac{sin(2sd)}{2s}\right]}{[cosh(2rd) - cos(2sd)]}\right\}$ represents the correction factor due to the depth of penetration.

Verification aspects

In order to verify the analysis results, the produced eddy current density and power are compared with that of the system presented in [11]. That system was analyzed numerically by using the finite-element representation of the ANSYS program. The induced eddy current density, at the centre point of the workpiece, obtained by the analytical method is shown in Figure-10 as conjunction with that of the numerical method with a variation of strip thickness. Also, the same comparison with a variation of air-gap is shown in Figure-11. Moreover, the produced averaged power within the strip is depicted in Figure (12) and (13) as compared with that of the numerical method due to the thickness and air-gap variation respectively. Obviously, the results show significant convergence between mathematical analysis method and numerical analysis method.

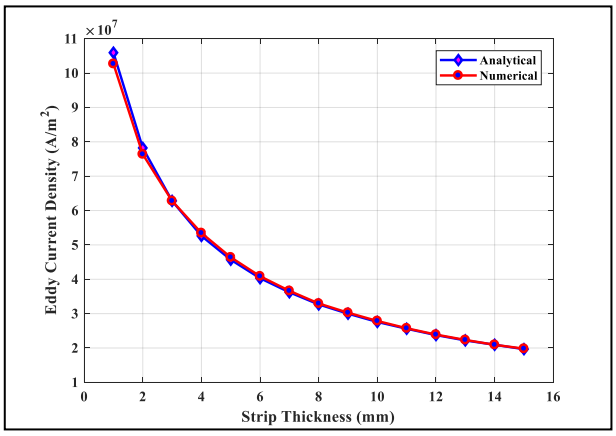

Figure-10. The eddy current densities with material thickness variation.

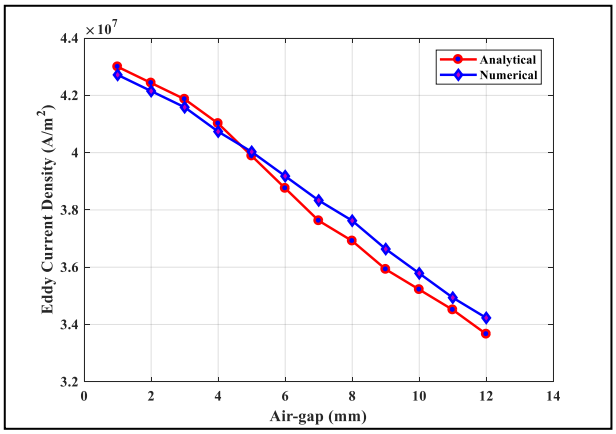

Figure-11. The eddy current densities with air-gap variation.

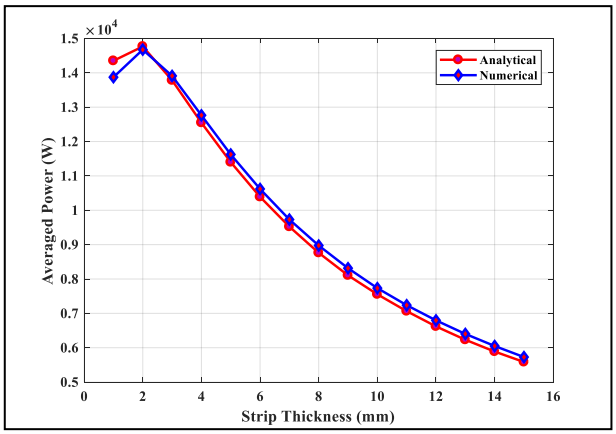

Figure-12. The averaged produced power with material thickness variation.

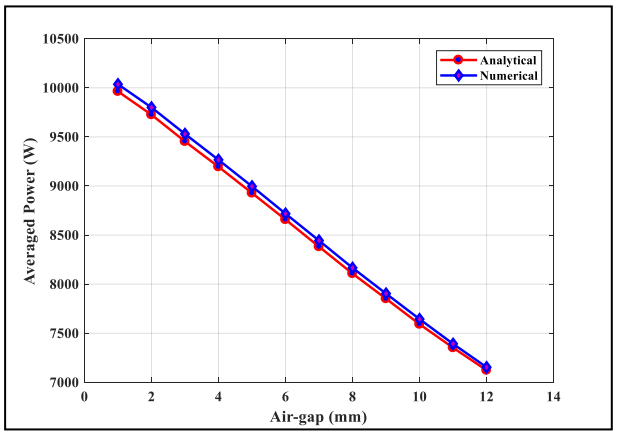

Figure-13. The averaged produced power with air-gap variation.

CONCLUSIONS

This paper presents the analysis and the mathematical model, of the TWIH system, in the two-dimensional coordinate to investigate the electromagnetic field quantities for both of the heater and heated workpiece. By the 2-D model, the conception of the TWIH theory was derived by determining the parameters of the electromagnetic problem within the heating system. The solution of the electromagnetic field was involved in the behaviour of the magnetic field attenuation, material impedance, normal forces between the heater and material, the air-gap flux, magnetizing reactance and effective workpiece resistance. Simulation results show significant convergence between the presented analytical method and the numerical analysis method. The percentage errors between the two methods, for both of eddy current density and averaged power, are very acceptable for major analysis requirements. The proposed model can replace the numerical model in an efficient manner in terms of the accuracy of the results in addition to reducing the computation time and the provision of effort in building the numerical model.

REFERENCES

[1] B. A. Nasir. 1997. Theory and Design of Travelling Wave Induction Heaters for Flat Metallic Workpieces. PhD. Thesis, Al-Mustansiriyah University, March.

[2] V. Rudnev, D. loveless, R. Cook and M. Black. 2003. Handbook of Induction Heating. M. Dekker Inc., New York, USA.

[3] Lingling Pang, Youhua Wang and Tanggong Chen. 2010. New Development of Traveling Wave Induction Heating. IEEE Transactions on Applied Superconductivity. 20(3).

[4] Guillermo Martn Segura. 2012. Induction Heating Converter's Design, Control and Modeling Applied to

Continuous Wire Heating. PhD Thesis, technical university of Catalonia.

[5] Z. Popovic and B. D. Popovic. 2012. Introductory Electromagnetics. Prentice Hall, Inc., Version 12.

[6] Ashutosh Pramanik. 2009. Electromagnetism Theory and Applications. PHI Learning Private Limited, 2nd Edition.

[7] Junhua Wang, Youhua Wang, S. L.Ho, Xiaoguang Yang, W. N. Fu and Guizhi Xu. 2011. Design and FEM Analysis of a New Distributed Vernier Traveling Wave Induction Heater for Heating Moving Thin Strips. IEEE Transactions on Magnetics. 47(10).

[8] Kenneth Frogner, Tord Cedell and Mats Andersson. 2014. Decoupling of Current in Travelling Wave Induction Heating. Journal of Electromagnetic Analysis and Applications. pp. 193-202, 6.

[9] B. Klimpke and C. Rebizant. 1997. Two and Three Dimensional Coupled Electromagnetic/Thermal Analysis for Induction Heating Application Using the Boundary Element Method (BEM). Integrated Engineering Software, February.

[10] S. Zinn and S. L. Semiatin. 1988. Elements of Induction Heating - Design, Control, and Applications. ASM International, Electronic Power Research Institute, Metals Park, Ohio, USA.

[11] A. K. Al-shaikhli, A. T. Humod and F. Abbas. 2015. Closed and quasi-closed yoke configurations for travelling wave induction heaters. IET, the Journal of Engineering. 2015(12): 357-363, 12. doi: 10.1049/joe.2015.0147.